

Electrochemical and photoelectrochemical characterization of CuFeO_2 single crystal

S. Omeiri · B. Bellal · A. Bouguelia · Y. Bessekhoud · M. Trari

Received: 19 July 2008 / Revised: 4 October 2008 / Accepted: 7 October 2008 / Published online: 21 October 2008
© Springer-Verlag 2008

Abstract CuFeO_2 single crystal, synthesized by the flux method, is a narrow band gap semiconductor crystallizing in the delafossite structure with a direct optical transition of 1.63 eV. The oxide exhibits a good chemical stability; the semi-logarithmic plot gave an exchange current density of $0.60 \mu\text{A cm}^{-2}$ in KCl (0.5 M) electrolyte. CuFeO_2 shows p -type conductivity; the origin of acceptors Cu^{2+} results from oxygen insertion in the layered lattice where most of excess holes are trapped in surface-polaron states. The electrochemical study is confined in the (a,b) plane and reversible oxygen intercalation is evidenced from the intensity potential characteristics. The detailed photoelectrochemical studies have been reported for the first time on the single crystal. The photocurrent is ascribed to the transfer $\text{Cu}^+ : 3d \rightarrow 3d$. The capacitance measurement ($C^{-2}-V$) shows a linear behavior from which a flat band potential of $+0.54 \text{ V}_{\text{SCE}}$ and a density N_A of $1.60 \times 10^{18} \text{ cm}^{-3}$ were determined. The valence band, located at 5.33 eV below vacuum, is made up of Cu-3d orbital typical of delafossite oxides. The Nyquist plot shows a semicircle attributed to a capacitive behavior with a low density of surface states within the gap. The centre is localized below the real axis with an angle of 16.2° ascribed to a constant phase element (CPE), a single barrier of the junction $\text{CuFeO}_2/\text{electrolyte}$ and one relaxation time of the electrical equivalent circuit.

Keywords CuFeO_2 · Single crystal · Semiconductor · Photoelectrochemical · Electrochemical impedance spectroscopy

Introduction

The development of new electrode materials for the conversion of the light-to-electrical and/or chemical energy has been extensively investigated and remains still the subject of intensive researches [1, 2]. Many oxides like TiO_2 or WO_3 have been studied for the water photosplitting because of their chemical inertness [3]. However, the major hindrance restricting their utilization in photoelectrochemistry remains the wide optical gap (E_g) where the photosensitivity is limited to UV radiation. The main cause is that the low lying valence band (VB) deriving from $\text{O}^{2-} : 2p$ orbital lies too deep in energy ($\sim -7 \text{ eV/vacuum}$). Hence, the conduction band (CB) generally consists of cationic parentage with a potential not negative enough to provide photo electrons with a reducing ability [4]. Some strategies have been attempted to overcome this drawback and our efforts have been focused on the oxides with new crystalline and band structure. The delafossites $\text{Cu}^+\text{M}^{3+}\text{O}_2$, where M is a 3d metal, represent an interesting family and emerged as having great promise for the photo photoelectrochemical (PEC) devices [5]. Non stoichiometry in CuMO_2 affects the transport properties which can be modulated by either thermal [6] or electrochemical oxygen insertion. This allows the oxide to be used for PEC characterization. In delafossites, both VB and CB are made up from Cu-3d wave function, the ion M^{3+} is electronically inactive and plays no direct role in the energy band diagram [7]. This should therefore slow down the corrosion process owing to the layered crystal structure and p type conductivity. Upon

S. Omeiri · B. Bellal · A. Bouguelia · Y. Bessekhoud · M. Trari (✉)
Laboratory of Storage and Valorization of Renewable Energies,
Faculty of Chemistry, USTHB,
P.O. Box 32, 16111 Algiers, Algeria
e-mail: labosver@gmail.com

S. Omeiri
Technical and Scientific Research Center of Physical Analysis,
P.O. Box 248, 16004 Algiers, Algeria

illumination and in presence of appropriate reducing agents, CuMO_2 are remarkably stable and have proved to be quite promising with regard to the constancy in photocurrent output [8]. The further advantage with such oxides is that the flat band potential (V_{fb}) does not depend on pH. Hence, the electronic bands can be appropriately matched to redox levels in solution. We have taken advantage of this characteristic and the PEC properties towards the water decomposition and the metals deposition have yet been exploited [9]. At a given pH, CB is suitably positioned with respect to the $\text{H}_2\text{O}/\text{H}_2$ level and the photoelectrons reduce spontaneously water into gaseous hydrogen without any external bias [10]. CuFeO_2 is one of the most stable oxides in the ternary system Cu–Fe–O. However whereas the physical properties have been studied [11], to our knowledge, no previous electrochemical study on the single crystal has been reported and the detailed PEC properties do not form any previous investigation. The structure is highly anisotropic and the electrochemical study is confined in the basal plane. The present work deals with the synthesis of CuFeO_2 single crystals by the flux method, the electrochemical properties and PEC characterization. Therefore an interesting question arises: does the electrochemical characterization qualify for the two dimensional model.

Experimental

Preparation of ceramic

CuFeO_2 powder has been synthesized through nitrate way as reported in our previous work [8]; unreacted Cu_2O was removed by soaking the powder in NH_4OH (5N). The end product exhibits a dark blue color and X-ray powder pattern, taken with Cu $K\alpha$ radiation revealed single phase (Fig. 1).

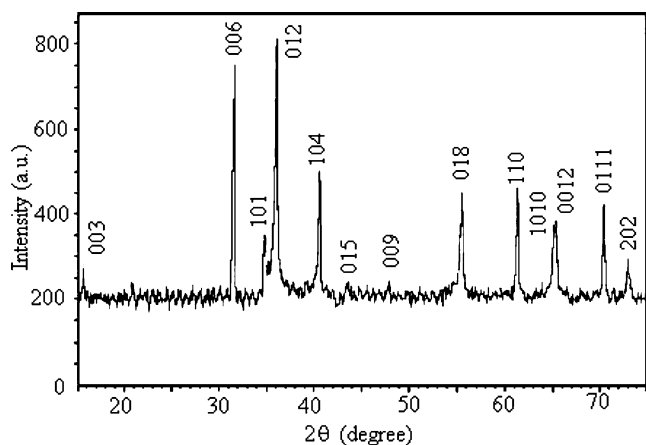


Fig. 1 XRD pattern of CuFeO_2 powder, elaborated by nitrate route

Single crystal growth

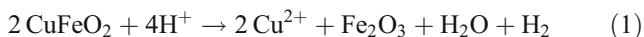
From the phase diagram Cu–Fe–O [12], one can anticipate the formation of CuFeO_2 in the Cu rich side. The crystals were grown using Cu_2O flux with a slightly modified method described elsewhere [13]. The synthesis has been performed under argon flow in a platinum crucible standing in a vertical programming furnace (Linn High Term). A mixture of extra pure CuO and Fe_2O_3 (30 g) was heated at $1,160^\circ\text{C}$ ($60^\circ\text{C}/\text{h}$) and maintained 12 h at that temperature. The cooling rate (1.5 K s^{-1}) was controlled from $1,140$ to 700°C below which the sample follows the natural cooling. The crystals appear black mirror like in reflected daylight and their length lies between 1 and 2 mm. The back electrical contact on (001) oriented single crystal was made with In–Ga alloy. The conductivity and the thermopower have been measured at room temperature in home hold equipments.

The crystals were inserted in glass holders with insulating epoxy. For the polarization curves and impedances measurements, a conventional three electrode set up has been employed. High purity platinum (5 N, 1 cm^2) etched in concentrated HCl, served as auxiliary electrode. The electrode potentials were monitored by a Voltalab PGZ301 potentiostat and scaled against a saturated calomel electrode. The supporting electrolyte (KOH 1 M), used for its high electro conductivity, was continually desaturated by bubbling with nitrogen. The capacitance was measured as a function of the potential with a scan rate of 10 mV step^{-1} . AC voltage signal of 10 kHz in frequency and 10 mV peak to peak in magnitude was applied to the system. To facilitate the light transmission, the working electrode was irradiated through a flat quartz window by a 500-W halogen lamp (Osram) whose output was passed trough a monochromator with 10-nm band pass. The light intensity was measured with a calibrated radiometer (model Testo 545) positioned at the same position of the electrode. The solutions have been prepared from reagents of analytical quality and deionized water.

Results and discussion

CuFeO_2 melts peritectically and the flux method appeared appropriate for the elaboration of single crystals. For the corrosion study, the amount of dissolved crystals would have been too small for a reliable determination of Cu^{2+} . However, with powder, long-term chemical stability was carried out for up to 6 months continuous operation. Cu^+ is less oxidant than Fe^{3+} and in the crystal lattice; the formulation ($\text{Cu}^+/\text{Fe}^{3+}$) is counterbalanced by the reticular energy. In the electrochemistry of semiconductors, the corrosion is important to investigate owing to its negative

aspect with respect to the PEC applications. CuFeO₂ was studied in various solutions spanning a wide pH range. It dissolves very slowly in acids, and the corrosion rate increases approximately linearly in a logarithm scale with decreasing pH. It was evaluated by analyzing both dissolved copper and iron by inductively coupled plasma and the results are illustrated in Fig. 2. In acidic media, the dissolution of copper is about ten times greater than that of iron; this can be understood by the low solubility of Fe₂O₃ according to the reaction:



with a standard free energy ($\Delta G_{298\text{K}}=69.8 \text{ kJ mol}^{-1}$) [14]. The corrosion study was confirmed independently, (Fig. 2, Insert) shows the semi logarithmic plots of the single crystal at various pH and the main electrokinetic parameters are gathered in Table 1. If anodically stable, CuFeO₂ must have a dissolution potential cathodic of the redox couple. It approaches 100 % stability to photocorrosion in presence of reducing agents such as S₂O₃²⁻. The chemical stability is attributed to the fact that the electronic states of the highest VB, in which the reacting holes are generated, are made up of Cu-3d orbital which are non bonding states in the theoretical description.

CuFeO₂ crystallizes in a rhombohedral structure with the space group R $\bar{3}m(D_{3d}^5)$. The XRD profile of the powder, depicted in Fig. 1, reveals a single phase. The refined lattice constants $a_h=0.3033$ and $c_h=1.7136$ nm are in perfect agreement with those previously reported where the authors also gave a detailed crystal structure of the polytype 3R-CuFeO₂ [15]. The FeO₆ octahedral units share common edges in the basal plane forming a two dimensional lattice

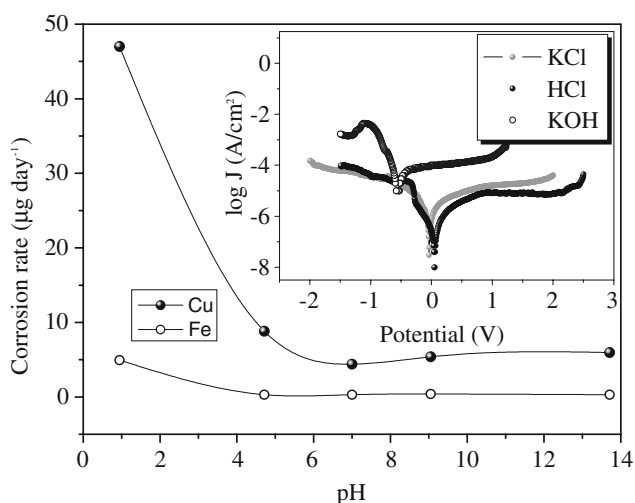


Fig. 2 The pH dependence of the corrosion rate of CuFeO₂. *Insert:* Semi logarithmic plots of CuFeO₂ single crystal in various electrolytes (0.5 M)

Table 1 Kinetic parameters of corrosion process for CuFeO₂ in various solutions

Electrolyte (0.5 M)	HCl	KCl	NaOH
J_0 ($\mu\text{A cm}^{-2}$)	0.20	0.62	1.03
Corrosion potential (V)	+0.053	-0.027	+0.215
Polarization resistance ($\text{k}\Omega \text{ cm}^2$)	231.65	62.01	192.09
Corrosion rate ($\mu\text{mol/year}$)	-0.289	-0.329	-0.330

giving and CuFeO₂ anisotropic properties. Octahedra, belonging to two adjacent layers, are linked to each other by linear CuO₂³⁻ entities parallel to *c* axis. CB consists of empty hybridized 4s/2p orbital whereas the lower non bonding *t*_{2g} orbital constitutes VB [16]; this energetic scheme agrees with the semi conducting behavior. Indeed, Cu⁺ has a *d*¹⁰ closed shell configuration and CuFeO₂ is expected to be semiconductor. The inter-ionic distance Cu⁺-Cu⁺ (0.3033 nm), equal to *a* parameter, is larger than the critical cation of 3d overlap for collective electrons (0.1241 nm)². However, the transport properties of CuFeO₂ depend on the deviation from the stoichiometry and are governed mainly by the oxygen insertion in the layered lattice. This should be accompanied by a partial oxidation of copper and the oxide is accurately formulated as Cu_{1-2δ}⁺Cu_{2δ}²⁺Fe³⁺O_{2+δ} considering the electro neutrality condition. The holes concentration is based on a charge balance on the assumption that each inserted O²⁻ yields two holes. The small amount of intercalated oxygen is readily understood in terms of coordination polyhedra. From a crystallochemical point of view, Cu²⁺ does not enjoy linear coordination without local deformation; it adopts rather octahedral fold coordination [17]. The conductivity is highly anisotropic, being much greater perpendicular to the *c* axis in which plane is lower to that of copper. Its value ($\sigma_{300\text{K}}=1.9 \times 10^{-3} \Omega^{-1} \text{ cm}^{-1}$) and the thermopower ($S_{300\text{K}}=157 \mu\text{V K}^{-1}$) indicate that the conduction occurs predominantly by small polaron hopping through mixed valences Cu⁺²⁺. In such a case, *S* is given by:

$$S = \left(\frac{k}{e}\right) \frac{\Delta E_{\perp}}{kT} = \left(\frac{k}{e}\right) \ln\left(\frac{N_0}{N_A}\right) \quad (2)$$

*N*₀ is the density of available sites, assimilated to the Cu⁺ concentration ($2.07 \times 10^{22} \text{ cm}^{-3}$) and calculated from the experimental density (5.20 g cm^{-3}). *N*_A is the density of polarons taking part in the conduction process (see below). The *S* value yields an activation energy ΔE_{\perp} in the (a, b) plane of 47 meV, very close to that given in the literature [13] and a ratio *N*_A/*N*₀ of 16 %. Hence, nearly all Cu²⁺ acceptors are localized at room temperature. The holes move in the narrow Cu-3d band, not exceeding 2 eV width,

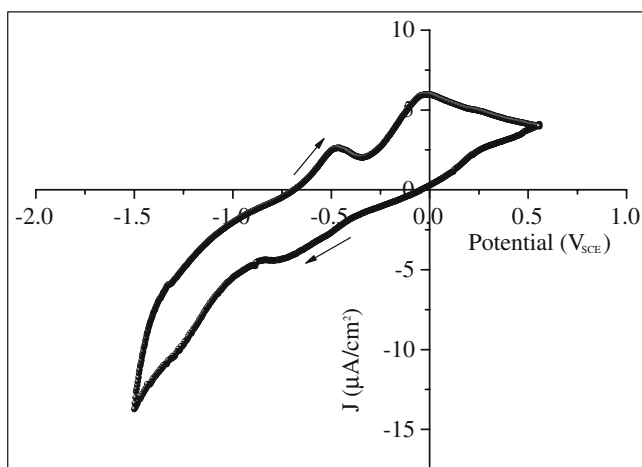


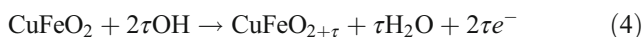
Fig. 3 The cyclic voltammogram of CuFeO₂ single crystal in the dark under nitrogen; electrolyte: KOH (0.5 M), scan rate 10 mV s⁻¹

and the mobility μ_h is expected to be low; μ_h was calculated from the formula:

$$\sigma = e\mu_h N_A \quad (3)$$

it was found to be $6.87 \times 10^{-3} \text{ cm}^2 \text{ V}^{-1} \text{ s}^{-1}$.

CuFeO₂ is an interesting material for PEC characterization and the suitable position of the electronic bands make the single crystal important to explore, the (001) face has been used as active area. In KOH electrolyte (pH 13.4), the free potential (-0.33 V) belongs to the immunity domain in the potential-pH diagram [14]. A typical cyclic $J(V)$ profile indicates a rectifying junction at the electrolyte contact with a dark current J_d less than $5 \mu\text{A cm}^{-2}$ and a good electrochemical stability (Fig. 3), the nature of the potential barrier is considered to be of Schottky type. Further support of the localization of holes is brought by the existence of the peak corresponding to the electrochemical couple Cu^{+2/+}. The layered structure can accommodate oxygen by electrochemical oxidation and the anodic peak at ~ -0.47 V is originated from O²⁻ intercalation [18]. Electrons are coming out from the Cu₂O planes inducing mixed valences Cu^{+2/+}. Taking into account the charge neutrality, the electrochemical reaction can be written:



where τ stands for the amount of incorporated oxygen. The charge under the anodic peak, measured by area integration, is evaluated to $\sim 4 \text{ mC cm}^{-2}$ and corresponds to the oxidation of $\sim 2.5 \times 10^{16} \text{ at. Cu}^+ \text{ cm}^{-2}$. A second peak located at ~ 0 V may be attributed to the oxidation Cu^{2+/3+}. On the reverse scan, the oxide undergoes reductions at ~ -0.13 and -0.74 V followed subsequently by the oxygen deintercalation. On a more qualitative point of view, a fast electron transfer (reversible system) is characterized by a separation between the peaks of $0.06/n$. However, the large difference exceeding 0.3 V indicates a slow oxygen insertion–desinsertion. The

electrons flow is faster, and the O²⁻ diffusion is rate-determining step in such process. Below -0.9 V, the current shoots up considerably due to H₂ evolution (gas bubbles are noticeable on the electrode).

The separation of the electron–hole (e^-/h^+) pairs is achieved by the junction electric field developed across the depletion width. The increase of the photocurrent J_{ph} along the negative polarization (Fig. 4) is consistent with p -type conductivity and provides an evidence of a space charge region. The constancy of the photocurrent under vigorous agitation of the solution indicates that the whole PEC process is controlled exclusively by the electron flow within the diffusion length and the ions transport does not affect the reaction rate. The slow decrease of J_d on illumination shutdown corroborates this hypothesis. At sufficient negative potentials, J_{ph} reaches a limiting value, the magnitude of which was found to depend only on the light intensity.

As noticed above, both the bands HOMO (VB) and LUMO (CB) are predominantly Cu-3d orbital in character with a separation characterized by the strength of the ligand field and which averages 2 eV. Cu⁺ is linearly coordinated and only one type of charge transfer (Cu⁺ → Cu⁺) can be involved in the energy range considered. The transition (O_{tetr}²⁻ + Fe_{oct}³⁺ → O_{tetr}⁻ + Fe_{oct}²⁺) occurs at energy higher than 4 eV. The spectral photo response has been measured in the range 400–1,000 nm using a grating monochromator with a band width of 10 nm. The quantum yield (η) is given by [19]:

$$(\eta h\nu)^m = A(h\nu - Eg) \quad (5)$$

m is equal to 2 or 1/2, respectively, for direct and indirect optical transitions. The plot of $(\eta h\nu)^m$ against $h\nu$ permits the determination of Eg and the nature of the transition; η was determined by dividing the electron flow in the

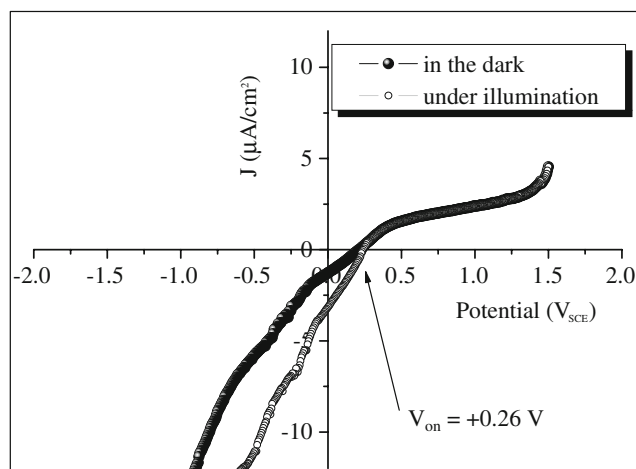


Fig. 4 $J(V)$ characteristics of p -type CuFeO₂ single crystal in KOH (0.5 M) both *in the dark* and *under illumination*, scan rate 10 mV s⁻¹

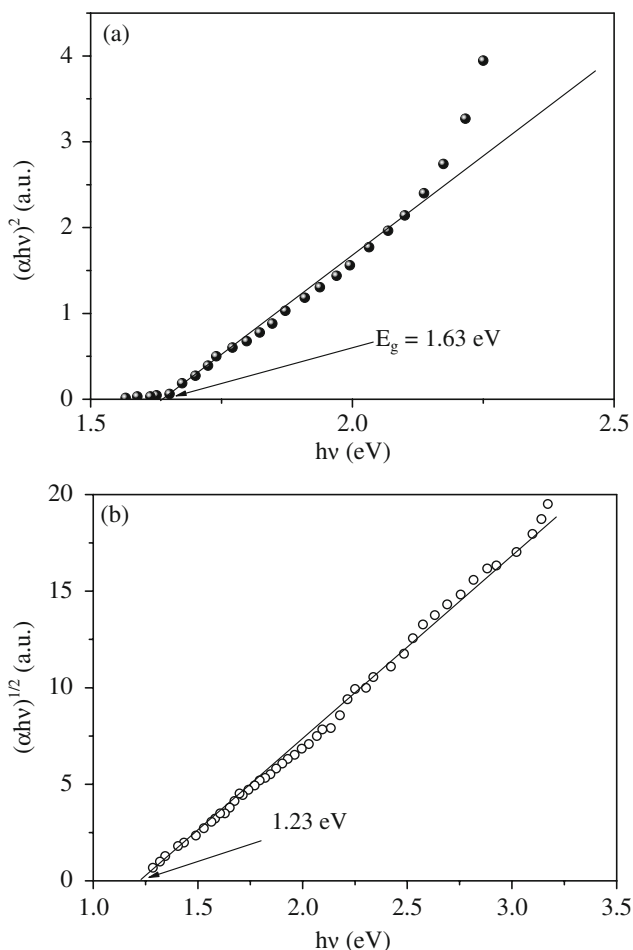


Fig. 5 Determination of direct (a) and indirect (b) optical interband transitions of CuFeO₂ single crystal

external circuit (photocurrent) by the incident photons flux (Φ_0) determined with a calibrated photodiode at each wavelength:

$$\eta = \frac{(J_{ph} - J_d)}{\Phi_0} \tag{6}$$

The intercept of the linear plot of $(\eta hv)^1$ with the hv -axis (Fig. 5) yields E_g value of 1.63 eV and the transition is directly allowed ($m=2$). A further transition indirectly allowed ($m=0.5$) and phonon assisted occurs at 1.23 eV.

The transient photocurrent-onset-potential (V_{on}), at which J_{ph} appears, is equal to +0.26 V (Fig. 4) in either solution indicating no preferential adsorption of H_3O^+ or OH^- on the electrode surface. V_{on} does not change significantly with pH because of the cationic character of the electronic bands. It should be mentioned that J_{ph} starts

¹ Calculated from the lattice constant (0.3885 nm) of iron crystallizing in a face centered cubic lattice.

to flow with a certain overvoltage depending on the surface states within the gap region. To get the potential V_{fb} , we used the relation:

$$J_{ph}^2 = \text{const.} \alpha^2 \delta^2 (V_{fb} - V) \tag{7}$$

α being the optical absorption coefficient and δ the depletion width. If $\alpha \delta (V - V_{fb})^{1/2} \ll 1$, the linear plot of J_{ph}^2 intercept the V-axis at the potential V_{fb} equal in our case to +0.56 V (Fig. 6, Insert). However, the potential V_{fb} has been accurately determined from the capacitance measurement:

$$C^{-1} = C_H^{-1} + C_{SC}^{-1} \tag{8}$$

where C_H is the Helmholtz capacitance and C_{SC} is the space charge capacitance. Due to the small conductivity of CuFeO₂, the parasitic inductance can be ignored even at low frequencies. The approximation $C_H \gamma \tau; \gamma \tau; C_{SC}$ is valid and the term $(1/C_H)$ can be neglected [20]. In addition, the frequency set at 10 kHz is large enough that the capacity of the space charge region dominates the global capacitance and C_{sc} is given by the well known formula:

$$\frac{1}{C_{SC}^2} = \pm \frac{2}{e \epsilon \epsilon_0 A N_A} \left(V - V_{fb} - \frac{kT}{e} \right) \tag{9}$$

where A is the surface area and the other symbols have their usual meaning. The positive sign is for n type and the negative sign for p type conductivity. The potential V_{fb} (+0.54 V) is obtained from the intercept of the plot to $C^{-2}=0$ (Fig. 6). It is only slightly larger than V_{on} and this indicates a quasi absence of surface states. V_{fb} measures the potential

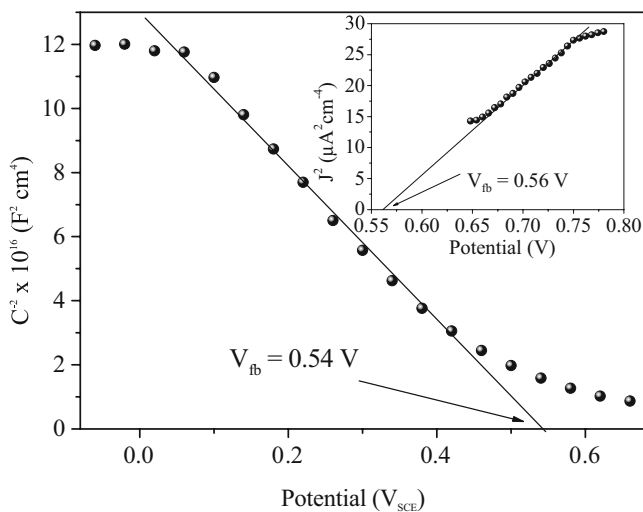


Fig. 6 The Mott-Schottky plot of p -type CuFeO₂ single crystal in KOH (0.5 M), the frequency was set up at 20 kHz. *Insert:* The accurate determination of the potential V_{fb} through the Butler relation (see text)

Table 2 Main characteristics of CuFeO₂

	σ ($\Omega^{-1} \text{ cm}^{-1}$)	μ ($\text{cm}^2/\text{V s}$)	$N_A \times 10^{-20}$ (cm^{-3})	V_{fb} (V)	δ^a (nm)	Source
Single crystal	1.9×10^{-3}	7.42×10^{-3}	0.016	+0.54	204	This work
	96	34	18			[13]
Polycrystal	3.25×10^{-4}	5×10^{-5}	0.41	0.16	40	This work
	1.9×10^{-5}	10^{-6}	1.20	~0		[13, 21]
	1.53	0.27	0.39			[21]

^a Calculated for a band bending of 0.5 V

required to completely remove the band bending at the interface. The linear behavior ($C^{-2}-V$) indicates a uniform density N_A of acceptors ($1.60 \times 10^{18} \text{ cm}^{-3}$), determined from $2(\epsilon\epsilon_0 \times \text{slope})^{-1}$. The bending over the curve (>0.6 V) implies a predominance of the recombination process when one approaches the potential V_{fb} from below i.e. the flat band conditions. The negative slope and the positive potential V_{fb} confirm the p type character of the single crystal. The permittivity (ϵ) is not available in the literature; its value ($\sim 1,200$) has been determined independently from the dielectric measurement on the polycrystal. The low N_A value characterizes non degenerate semi conductivity, responsible of a large depletion width (~ 200 nm) evaluated for a band bending of 0.5 V through the relation [21]:

$$\delta = \left\{ \frac{2\epsilon\epsilon_0(V - V_{fb})}{eN_A} \right\}^{0.5} \quad (10)$$

A correlation exists between the theoretical electron affinity (EA_{the}) of the semiconductor, its electro negativity (χ) and Eg^2 [22]:

$$EA_{the} = \chi(\text{CuFeO}_2) + 0.5Eg \quad (11)$$

The $pzzp$ (7.36) is the pH at which the net charge of adsorbed ions on the surface is zero, it is the only pH at which the meaningful potential V_{fb} can be determined and EA_{the} is found to be 5.06 eV. On the other hand, the experimental electro affinity (EA_{exp}) is given by:

$$EA_{exp} = 4.75 - eV_{fb}(pzzp) - \Delta E_{\perp} + \Delta pH \quad (12)$$

ΔpH is the potential drop across the Helmholtz layer due to specific adsorption of H_3O^+ and OH^- and at $pzzp$ it is equal to zero. The EA_{exp} value (4.21 eV) is typical of materials in which CB is made by hybridized Cu-3d-4s [7]. The discrepancy between EA_{exp} and EA_{the} indicates that the relation (11) gives a rough approximation of the electron

² χ is the geometrical mean of EA values of the constituent atoms, $\chi(\text{CuFeO}_2) = \{(\chi_{\text{Cu}})(\chi_{\text{Fe}})(\chi_{\text{O}})^2\}^{1/4}$. For a neutral atom, χ is given by $(A_f + I_1)/2$ where A_f is the electron affinity and I_1 the first ionization energy, the values were taken from [23].

affinity of SC compounds. The physical parameters are gathered in Table 2 for comparative study.

Much can be learned from the electrochemical impedance spectroscopy (EIS). The measurement of the junction CuFeO₂/solution, performed at the open circuit potential (OCP, -0.283 V), allows to distinguish between the various mechanisms and to propose an equivalent circuit. The direct exchange of majority carriers occurs through the interface and is represented by the Nyquist plot (Fig. 7) whose nature confirms the predominance of the bulk contribution. The arc at high frequencies is attributed to a faradic charge transfer and the extrapolation with the x axis lead to the corresponding resistance (R_{dl}). The parameters were refined by the least square method between the real and imaginary impedances Z' and Z'' with the experimental data. The system is under kinetic control and the resistance R_{dl} ($12.41 \text{ k}\Omega \text{ cm}^2$) is in parallel with the capacitance C_{dl} (35.88 nF cm^{-2}). We also note a slight offset near the origin indicating a low series resistance ($630 \Omega \text{ cm}^2$) attributed to both the electrolyte and the electrode R_{el} itself. The centre of the arc is localized below the real axis with an angle of 16.2° ascribed to a constant phase element (CPE). Such behavior can be attributed to various phenomena such as surface states, the distribution of current and potential field

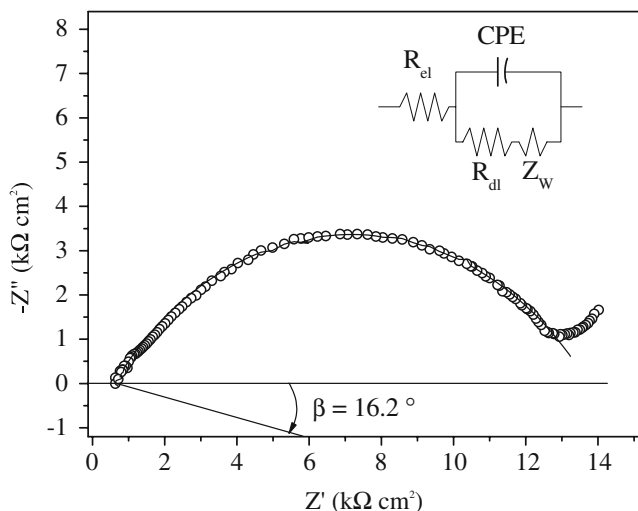


Fig. 7 The Nyquist plot of p -type CuFeO₂ single crystal in KOH (0.5 M). *Insert:* the corresponding equivalent electrical circuit

and slow adsorption [24]. The straight line at low frequencies is due to the diffusion of electroactive species in the solution known as the Warburg impedance (Z_w), which indicates that the anionic diffusion prevails over the electron transfer. Since the ionic diffusion and the heterogeneous charge transfer occur as successive mechanisms, the equivalent electrical circuit (Fig. 7, Insert) is composed of the impedance Z_w in series with the resistance R_{dl} which in turn are connected in parallel with CPE. Owing to the above properties, *p*-CuFeO₂ seems an attractive material for photovoltaic cells whether a liquid or the photo-electrochemical conversion solid junction.

Conclusion

The PEC properties of the delafossite CuFeO₂ have been reported for the first time on the single crystal. The oxide is classified as a narrow direct band semiconductor and Cu²⁺ is generated by oxygen insertion to conserve the electro neutrality. The order of magnitude of the conductivity and the thermopower confirm the semi conducting like properties. The electrochemical study was confined in the basal planes and the natural face of the hexagonal layered crystal perpendicular to the [001] direction has been selected as active surface. The reversibility of oxygen insertion was proven by the intensity potential characteristics. The spectral dependence of the quantum yield has been analyzed to give the energy of the inter band transitions. The PEC measurements indicated an upper valence band made up primarily of copper character located at ~5 eV below vacuum. The *p*-type conductivity was confirmed by the cathodic direction of the photocurrent. The flat band potential and the carrier density were determined from the Mott-Schottky plot. The semicircle in the Nyquist plot overlaps in one symmetrical arc centered below the real axis. It indicates the electric process has single relaxation time due to the contribution of the bulk single crystal and is exclusively under kinetic control.

Acknowledgement The authors are grateful to M. Younsi for valuable suggestions regarding to the corrosion measurements. Financial support of this work was provided the Faculty of Chemistry (Algiers).

References

- Hu CC, Nian JN, Teng H (2008) Sol Energy Mater Sol Cells 92:1071. doi:10.1016/j.solmat.2008.03.012
- Tai Y-W, Chen J-S, Yang C-C, Wan B-Z (2004) Catal Today 90:95. doi:10.1016/j.cattod.2004.04.054
- Gondal MA, Hameed A, Yamani ZH, Arfaj A (2004) Chem Phys Lett 385:111. doi:10.1016/j.cplett.2003.12.066
- Claverie J, Campet G, Conte D, Le flem G, Hagenmuller P (1983) Phys Status Solidi (a) 77:603. doi:10.1002/pssa.2210770224
- Saadi S, Bouguelia A, Derbal A, Trari M (2007) J photochem photobiol 187:97
- Elazhari M, Ammar A, Elaatimani M, Trari M, Doumerc JP (1997) Eur J Solid State Inorg Chem 34:503
- Prewitt CT, Shannon RD, Rogers DB (1971) Inorg Chem 10:719. doi:10.1021/ic50098a012
- Younsi M, Aider A, Bouguelia A, Trari M (2005) Sol Energy 78:574. doi:10.1016/j.solener.2004.01.012
- Omeiri S, Gabès Y, Bouguelia A, Trari M (2008) J Electroanal Chem 614:31. doi:10.1016/j.jelechem.2007.11.002
- Trari M, Bouguelia A, Bessekhouad Y (2006) Sol Energy Mater Sol Cells 90:190. doi:10.1016/j.solmat.2005.03.003
- Doumerc JP, Wichainchai A, Ammar A, Pouchard M, Hagenmuller P (1986) Mater Res Bull 121:745. doi:10.1016/0025-5408(86)90155-8
- Zhao TR, Takei H (1997) Mater Res Bull 32:1377. doi:10.1016/S0025-5408(97)00126-8
- Dordor P, Chaminade JP, Wichainchai A, Marquestaut E, Doumerc JP, Pouchard P, Hagenmuller P (1988) J Solid State Chem 75:105. doi:10.1016/0022-4596(88)90307-6
- Cubicciotti D (1988) NACE 44:875
- Mugnier E, Barnabé A, Tailhades P (2006) Solid State Ion 177:607. doi:10.1016/j.ssi.2005.11.026
- Ong KP, Bai K, Wu P (2008) J Alloy Comp 449(1-2):366. doi:10.1016/j.jallcom.2006.01.141
- Trari M, Topfer J, Dordor P, Grenier JC, Pouchard M, Doumerc JP (2005) J Solid State Chem 178:2751. doi:10.1016/j.jssc.2005.06.009
- Grenier JC, Wattiaux A, Lagueyte N, Park JC, Marquestaut E, Etourneau J, Pouchard M (1991) Physica C 173:139. doi:10.1016/0921-4534(91)90360-B
- Tauc J (1974) Amorphous and liquid semiconductors. Plenum, London
- Pollert E, Hejtmanek J, Doumerc JP, Claverie J, Hagenmuller P (1983) J Phys Chem Solids 44:273. doi:10.1016/0022-3697(83)90095-1
- Xia S-J, Zhou W-F (1995) Electrochim Acta 40:175. doi:10.1016/0013-4686(94)00280-E
- Butler MA, Ginley DS (1978) J Electrochem Soc 125:228. doi:10.1149/1.2131419
- Lide DR (1997, 1998) Handbook of chemistry and physics, 78th edn. McGraw-Hill, New York
- Barsoukov E, Macdonald JR (2005) Impedance spectroscopy, theory, experiment and applications, 2nd edn. Wiley, New York